ADVANCED ENERGY MATERIALS
www.advenergymat.de

Rational Design of a Photosystem I Photoanode for the Fabrication of Biophotovoltaic Devices

Panpan Wang, Fangyuan Zhao, Anna Frank, Sarra Zerria, Anna Lielpetere, Adrian Ruff, Marc M. Nowaczyk, Wolfgang Schuhmann, and Felipe Conzuelo**

Photosystem I (PSI), a robust and abundant biomolecule capable of delivering high-energy photoelectrons, has a great potential for the fabrication of light-driven semi-artificial bioelectrodes. Although possibilities have been explored in this regard, the true capabilities of this technology have not been achieved yet, particularly for their use as bioanodes. Here, the use of PSI Langmuir monolayers and their electrical wiring with specifically designed redox polymers is shown, ensuring an efficient mediated electron transfer as the basis for the fabrication of an advanced biophotoanode. The bioelectrode is rationally implemented and optimized for enabling the generation of substantial photocurrents of up to 17.6 µA cm^{-2} and is even capable of delivering photocurrents at potentials as low as −300 mV vs standard hydrogen electrode, surpassing the performance of comparable devices. To highlight the applicability of the developed light-driven bioanode, a biophotovoltaic cell is assembled in combination with a gas-breathing biocathode. The assembly operates in a single compartment cell and delivers considerable power outputs at large cell voltages. The implemented biophotoanode constitutes an important step toward the development of advanced biophotovoltaic devices.

1. Introduction

Photosystem I (PSI) is one of the key protein complexes driving oxygenic photosynthesis. Acting as a natural photodiode, it is capable of performing charge separation upon absorption of visible light. The specific advantages in terms of its high quantum efficiency, natural abundance, and robustness of the isolated protein complex[1] render PSI an outstanding biomolecule for the development of semi-artificial technologies for solar energy conversion. As a result, great interest has been devoted to implementing bioelectrochemical devices integrating PSI with a variety of electrodes to exploit the potential offered by this biomolecule.[2–4] After light-induced charge separation and internal electron transfer within PSI, a relatively long-lived intermediate state is obtained comprised of the photo-oxidized special chlorophyll pair (P_{700}^+) and the terminal Fe-S cluster in the reduced state (F_B^-).[5] The high quantum efficiency and ability to transfer electrons from and to a variety of natural as well as artificial electron donors and acceptors make PSI an exceptional light-driven electron pump. Thus, the high-energy electrons exiting PSI can be exploited for driving reduction reactions of interest.[6] An additional option is to harvest the high-energy electrons at the electrode surface and to take advantage of the largely negative potentials achieved for establishing a light-driven bioanode. In both cases, the photo-oxidized P_{700}^+ needs to be continually reduced for an effective and sustained photocurrent generation. This can be done by an effective wiring of the biomolecule to the electrode surface or by the use of a sacrificial electron donor in solution.[3]

For the fabrication of light-driven bioanodes, photosystem II (PSII) has been the photosynthetic protein complex of choice as it is the only biomolecule known to be able to perform light-induced water oxidation.[7] However, PSII suffers from severe and irreversible photodamage,[8] compromising the applicability of related biodevices due to their considerably limited lifetime. In addition, the cofactors involved in the extraction of electrons from PSII present a relatively high redox potential, restricting the open-circuit voltage achieved in combination with a given (bio)cathode. In contrast, PSI is a great candidate for the fabrication of light-driven bioanodes. Isolated PSI is remarkably more stable and delivers electrons at a negative potential. In addition, the light-induced reaction can be coupled with a variety of (bio) catalysts performing oxidation reactions that concomitantly

P. Wang, F. Zhao, S. Zerria, A. Lielpetere, A. Ruff,[+] W. Schuhmann, F. Conzuelo
Analytical Chemistry – Center for Electrochemical Sciences (CES)
Faculty of Chemistry and Biochemistry
Ruhr University Bochum
Universitätsstr. 150, D-44780 Bochum, Germany
E-mail: wolfgang.schuhmann@rub.de; felipe.conzuelo@rub.de
F. Zhao
College of Chemical Engineering
China University of Mining and Technology
Xuzhou, Jiangsu 221008, P. R. China
A. Frank, M. M. Nowaczyk
Plant Biochemistry – Molecular Mechanisms of Photosynthesis
Faculty of Biology and Biotechnology
Ruhr University Bochum
Universitätsstr. 150, D-44780 Bochum, Germany
The ORCID identification number(s) for the author(s) of this article can be found under https://doi.org/10.1002/aenm.202102858.

[+]Present address: PPG Deutschland Business Support GmbH, PPG Packaging Coatings EMEA, Erlenbrunnenstr. 20, D-72411 Bodelshausen, Germany

DOI: 10.1002/aenm.202102858

provide the electrons required for the reduction of the photooxidized protein complex. Nevertheless, the integration of PSI with electrodes for the fabrication of functional devices is challenging and frequently translates into low efficiencies in the performance of associated biophotoelectrodes.[9] In nature, PSI is embedded in the thylakoid membrane, which ensures an optimal functioning due to a proper orientation of the protein complex and physical separation of the terminal redox centers by the lipid bilayer. However, the use of isolated photosystems for the fabrication of semi-artificial bioelectrodes commonly causes the loss of those crucial advantages, leading to photocurrent generation only due to an imbalance in competing electron transfer processes within the modified electrode. As a result, the strategies followed until now for the fabrication of PSI-based biophotoanodes have shown considerable limitations for photocurrent generation, which is reflected in particular at negative applied potentials.[10–14] As depicted schematically in **Figure 1**, several situations deviating from the ideally envisaged electron-transfer pathway (Figure 1a) can compromise the performance of a PSI biophotoanode. The electrochemical species used to replenish electrons to the photoexcited PSI can be also wired with the electrode surface (Figure 1b), bypassing PSI, and causing the occurrence of a competing light-independent anodic reaction at more positive potentials. Moreover, the terminal redox centers are located at opposite sides of the protein complex, imposing the need for a proper orientation of PSI over the electrode surface to achieve an improved performance (Figure 1c).[15] Finally, the large potential difference between F_B^- and P_{700}^+ of ≈1.0 V, often causes the short-circuiting of at least a portion of the electrons exiting PSI[16] and consequently limits the photocurrent output by a diversion of the generated electrons to reduce the oxidized electron donor accumulated in close proximity to P_{700}^+ (Figure 1d).

Consequently, advanced electrode architectures are required to overcome these hurdles and realize the true potential of biophotovoltaic devices. In this regard, Langmuir–Blodgett (LB) monolayers of preferentially oriented photosynthetic reaction centers can be formed at the air/water interface and subsequently transferred onto the electrode surface.[17,18] As we have recently shown, PSI-LB monolayers can be interfaced with adequately designed redox polymers for adapted electrical communication at both ends of the immobilized photosystem, which had permitted the implementation of highly efficient PSI-based biophotocathodes.[19,20] In this work, we present the rational design and optimization of a novel PSI-based biophotoanode and its use for the fabrication of a biophotovoltaic device. The bioelectrode comprises an LB monolayer of photosynthetic protein complexes that is interfaced with a low-potential viologen-modified polymer, enabling the efficient mediated transfer of photogenerated electrons to the electrode surface at negative potentials. The other end of immobilized PSI is coupled with a second redox polymer integrating glucose oxidase (GOx), which is used as model biocatalyst for providing the electrons required for the reduction of P_{700}^+ at PSI. The implemented bioelectrode has been optimized for enhanced generated photocurrents, even at particularly negative potentials, highlighting the advantages of a PSI-based photoanode. A gas-breathing biocathode is used to complete the electrochemical cell, which is driven by glucose and molecular oxygen. The biophotovoltaic assembly is operated with both electrodes in a membrane-free single compartment cell and is able to provide substantial power outputs at large cell voltages.

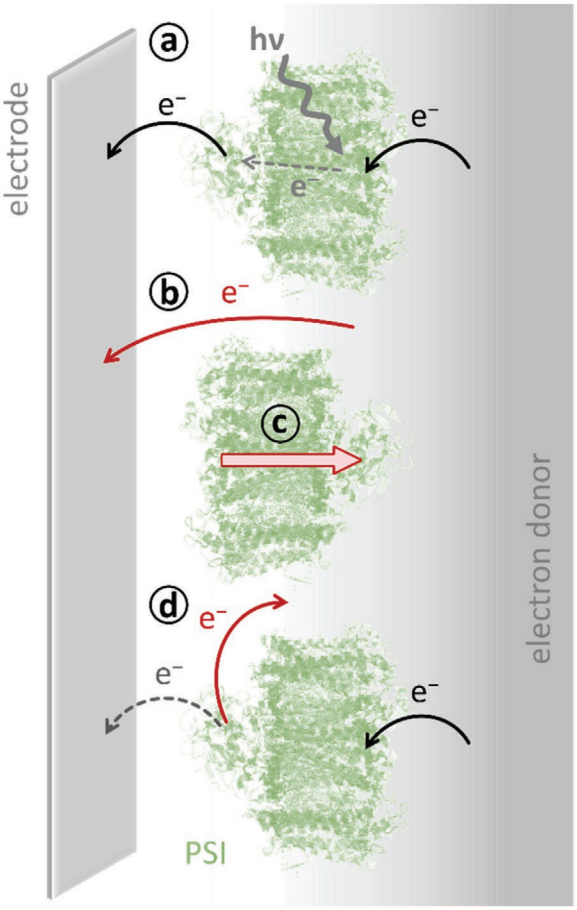

Figure 1. Electron transfer pathways involved in a photosystem I-based bioanode. a) In an ideal situation, after light-induced charge separation and internal electron transfer, the electrons exiting PSI are collected at the electrode, while an electron donor (sometimes in the presence of a suitable redox mediator) allows electron replenishment for sustained photocurrent generation. b) Direct oxidation of the electron donor or redox mediator over the electrode surface translates in PSI-independent current generation; thus, delivering electrons at much higher potentials. c) An uncontrolled orientation of immobilized PSI decreases the efficiency of the bioelectrode as only a portion of biomolecules contribute to photocurrent generation. d) Reduction of the oxidized electron donor or redox mediator by electrons exiting PSI results in a partial diversion of the generated photoelectrons into a short circuit, decreasing the number of electrons collected by the electrode.

2. Results and Discussion

2.1. Implementation of a Photosystem I-Based Bioanode

For the fabrication of a biophotoanode, the electrons exiting PSI are collected at the electrode surface. To establish a more efficient mediated electron transfer between the terminal F_B site at PSI and the electrode, a viologen-modified polymer (P-vio) was incorporated. The midpoint potential of P-vio (about −280 mV vs standard hydrogen electrode (SHE)[20,21]) ensured the necessary

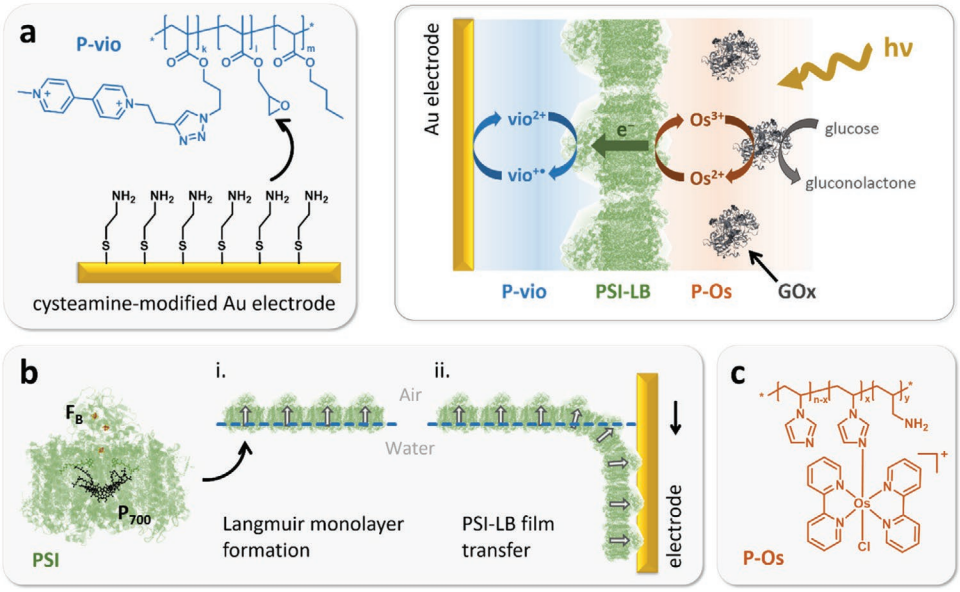

Figure 2. Schematic representation of the proposed PSI-based biophotoanode. a) Deposition of the viologen-modified polymer (P-vio) over the electrode surface previously modified with a monolayer of cysteamine. The amino functionalities react with epoxy groups at the polymer backbone for covalent attachment of the polymer film. b) Structure of a PSI protein complex highlighting its terminal redox centers. P_{700}: special chlorophyll pair, F_B: terminal Fe-S cluster. i) A monolayer of preferentially oriented PSI complexes is formed at the air/water interface. ii) Transfer of the PSI-LB film onto the electrode by dipping the substrate. The arrows indicate the orientation of the protein complexes in the direction $P_{700} \rightarrow F_B$. c) Structure of the Os-complex-modified redox polymer (P-Os) used as top modification layer. Elements not drawn to scale. PSI structure based on the protein data bank (PDB) entry 1JB0;[28] GOx structure based on the PDB entry 3QVR.[29]

driving force for promoting the extraction of electrons from PSI, exiting the terminal Fe-S cluster at a potential of −580 mV vs SHE. The Au electrode was first modified with a monolayer of cysteamine to attain sufficient stability of the rather hydrophilic polymer film. The amino functionalities can react with epoxy groups at the polymer backbone, resulting in the covalent attachment of the polymer film (**Figure 2**a). A potential pulse-assisted immobilization protocol was used to form the cysteamine monolayer over the electrode surface, enabling the controlled and reproducible formation of monolayer-modified electrodes in a short time.[22] Furthermore, branched polyethyleneimine (PEI) was used as crosslinking agent for attaining a stable tridimensional network of the viologen-modified polymer over the electrode. Following this approach, the surface coverage with P-vio was (52 ± 24) pmol cm^{-2} ($N = 3$ different electrodes), as inferred from the redox centers assessed by cyclic voltammetry according to the equation $\Gamma_{P\text{-vio}} = Q(nFA)^{-1}$, where Q is the charge for the redox conversion of the polymer-bound viologen units, n is the number of electrons transferred, F is the Faraday constant, and A is the geometric electrode area.

The electrode bearing the P-vio film was used for further deposition of a PSI-LB monolayer. As shown previously, the orientation of PSI over the electrode surface can be controlled by adjusting the direction of transfer of the PSI-LB film during deposition onto the electrode surface.[20] Therefore, for the fabrication of a PSI-based biophotoanode the deposition was performed by dipping the electrode substrate into the subphase of an LB trough where a compact monolayer of PSI has been previously formed (Figure 2b). As a result, the photosynthetic protein complexes were oriented with their F_B site toward the electrode surface. The resulting bioelectrode was investigated in the presence of ascorbate and dichlorophenolindophenol (DCPIP) as sacrificial electron donor and redox mediator, respectively, commonly used for replenishing of electrons at the PSI P_{700} site after light-induced charge separation.[3,4,11,12,14,18,23–27] The bioelectrode provided photocurrents of about 2.6 µA cm^{-2} at an applied potential (E_{app}) of 200 mV vs SHE (Figure S1a,c, Supporting Information). The rather modest response achieved could be attributed to a limitation in the kinetics for electron transfer as a result of the use of DCPIP as redox mediator, involving a $2e^-/2H^+$ redox interconversion. In addition, the use of a soluble redox mediator promotes the aforementioned short-circuiting pathway limiting the number of electrons collected at the electrode surface (see Figure 1d). Thus, a top layer consisting of an Os-complex-modified redox polymer (P-Os) was introduced, which ensured confinement of the redox mediator in a polymer layer and provided a more efficient electrical communication with the P_{700} site at PSI (Figure 2c). As a result, an improved performance was obtained, leading to photocurrent responses of 5.2 µA cm^{-2} (Figure S1b,d, Supporting Information). However, as observed in Figure S1 in the Supporting Information, negligible photocurrent responses were obtained in both cases at applied potentials more negative than 150 mV vs SHE, even in the presence of relatively large ascorbate concentrations. Note that the photocurrent response was dependent on the ascorbate concentration in the electrolyte solution and that lower photocurrents were obtained for concentrations below 40×10^{-3} M. In addition, the experimental results revealed that ascorbate could be directly oxidized at the electrode surface (Figure S2, Supporting Information), contributing to a substantial background current under dark conditions (see Figure S1, Supporting Information).

The use of a redox enzyme-catalyzed reaction to supply the electrons required for the reduction of P_{700}^+ was investigated. This possibility has been shown by coupling PSI with redox reactions driven by PSII,[11,30] GOx,[10] and human sulfite oxidase[31] and was further studied here for the fabrication of biophotoelectrodes with improved performance. GOx was deliberately selected for this purpose, as it can be effectively wired by P-Os in a mediated electron transfer configuration[32] and enables the use of glucose as electron source. Moreover, reduced GOx can be rapidly oxidized by molecular oxygen. Therefore, in addition to the supply of electrons for biophotoelectrode operation, the top modification layer can also serve as a protecting coating, where an excess of GOx is used for the removal of traces of O_2 that could otherwise compete with the electrode for the uptake of the high-energy electrons exiting PSI.

A schematic representation of the full bioelectrode is presented in Figure 2 (top right), which was able to deliver photocurrents of about 4.9 μA cm^{-2} (E_{app} = 200 mV vs SHE), a comparable response to that obtained when using ascorbate as sacrificial electron donor. Nevertheless, the large background current in the dark as a result of ascorbate oxidation could now be successfully suppressed. In addition, a substantially improved performance was observed at more negative applied potentials, leading to photocurrents of about 2.0 μA cm^{-2} at an applied potential as low as −200 mV vs SHE (**Figure 3**a). The influence of glucose concentration on the photoelectrode performance revealed no major differences when decreased down to 2 × 10^{-3} M (see Figure S3, Supporting Information), indicating that the bioelectrode was not limited by the supply of electrons to PSI. Furthermore, negligible photocurrents were observed in the absence of glucose (Figure 3b), confirming the role of glucose as sacrificial electron donor for enabling sustained photocurrent generation.

2.2. Bioelectrode Characterization

Different control experiments were performed to investigate and confirm the mechanism of photocurrent generation. First, a set of bioelectrodes was fabricated following the same procedure described previously but using the opposite direction of transfer during deposition of the PSI-LB film, which results in an orientation of the majority of the protein complexes with their F_B site away from the electrode surface. In this case, photocurrent responses in the order of 140 nA cm^{-2} were observed (E_{app} = 200 mV vs SHE, Figure S4a, Supporting Information), in contrast with an average of (5.0 ± 0.8) μA cm^{-2} (N = 3 different electrodes) for the optimal assembly (Figure 3c). This confirmed that the correct orientation of the photosynthetic protein complexes is crucial for photocurrent generation. Furthermore, a small photocurrent response of about 120 nA cm^{-2} was obtained with the PSI-LB film in the correct orientation but in the absence of the viologen-modified polymer, demonstrating that P-vio has a significant contribution to an efficient electrical

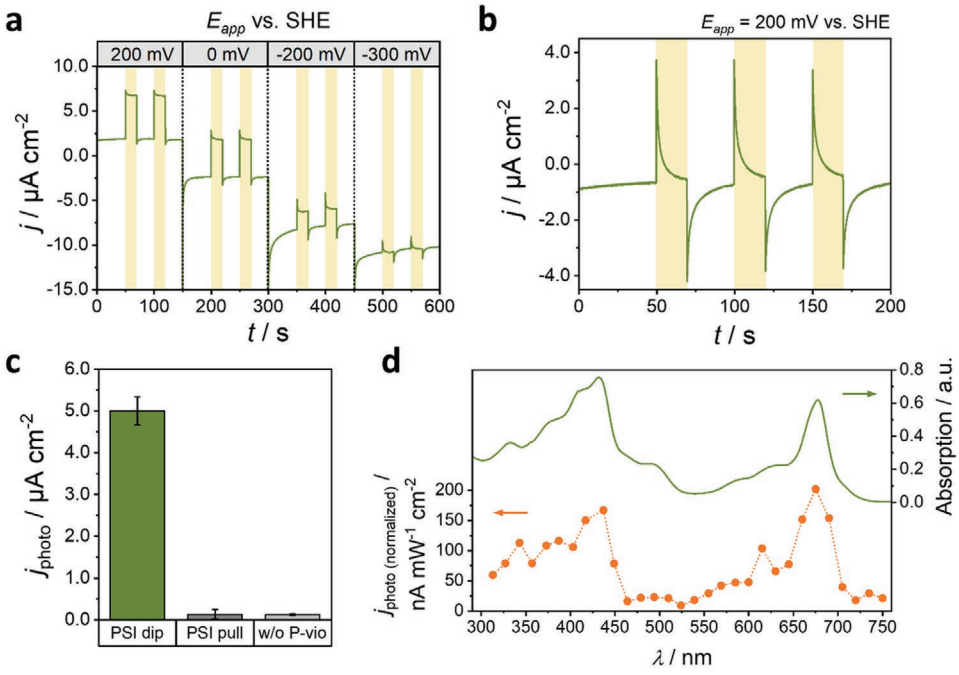

Figure 3. a) Representative photochronoamperometric measurement for a PSI-LB film over a P-vio-modified Au electrode with a top layer of GOx embedded in P-Os (Au/P-vio/PSI-LB/P-Os/GOx). Electrolyte: Ar-saturated 0.1 M phosphate buffer, pH 7.0, containing 10 × 10^{-3} M glucose. b) Measurement in the absence of glucose at E_{app} = 200 mV vs SHE. Illumination with white light during the times indicated by the yellow-shaded regions. c) Average of photocurrent responses at E_{app} = 200 mV vs SHE in the presence of 10 × 10^{-3} M glucose. PSI dip (N = 3 different electrodes prepared in the same manner): same electrode architecture as described in panel a. Control experiments (N = 2 different electrodes prepared in the same manner): PSI pull, electrode prepared using the opposite orientation for the PSI-LB monolayer; w/o P-vio, electrode prepared without the P-vio film. The error bars represent the standard deviation of the measurements. d) Comparison of the absorption spectrum obtained for isolated PSI in solution with the action spectrum for the fabricated biophotoelectrode calculated after the experimental data shown in Figure S5 in the Supporting Information.

wiring between the terminal F_B site at PSI and the electrode surface (cf. Figure 3a and Figure S4b, Supporting Information). Furthermore, to assess whether the photocurrent response is undoubtedly generated by PSI, the current output obtained with the biophotoelectrode was investigated under different irradiation wavelengths (Figure S5a, Supporting Information). As shown in Figure 3d, the resulting action spectrum was in agreement with the spectral features observed for the isolated photosystem, corroborating that the photocurrent response is caused by photoexcitation of immobilized PSI.

The high-energy electrons exiting PSI can reduce molecular oxygen in solution, consequently limiting the number of electrons reaching the electrode surface. Therefore, O_2-removal is highly relevant for the generation of anodic photocurrents with PSI-based bioelectrodes.[10,11,23,30] As shown in Figure S6a in the Supporting Information, the photocurrents attained under ambient conditions were approximately half of those recorded under Ar atmosphere, as a result of a partial diversion of the generated photoelectrons for the reduction of O_2. Nonetheless, the possibility to attain anodic photocurrents even in the presence of considerably high O_2 concentrations confirmed the capability of the GOx top modification layer for removing a large portion of O_2 before reaching the underlying bioassembly. Thus, the operation of the biophotoanode in the presence of minor O_2 concentrations was ensured (vide infra). This was confirmed after repeating the measurement under ambient conditions but in the absence of glucose. In this case, the direction of photocurrent was completely inverted, resulting in the appearance of cathodic photocurrents (Figure S6b, Supporting Information) as now O_2 could penetrate the film and act as the final electron acceptor instead of the electrode surface. Investigation of the long-term stability for bioelectrodes operated under an Ar atmosphere and in the presence of ambient air (Figure S7, Supporting Information) revealed the deleterious effect of H_2O_2 generated after O_2 consumption by GOx. While the bioelectrode operated under an Ar atmosphere retained 75% of the initial photocurrent after 90 min of intermittent illumination, the bioelectrode operated in the presence of ambient O_2 delivered less than 40% of the initial photocurrent. Therefore, negligible O_2 concentrations were necessary to ensure the maximum photocurrent output and stability of the bioelectrode.

2.3. Minimizing Short-Circuiting

Evaluation of the voltammetric response for the biophotoelectrode revealed that the start of the oxidation wave under illumination began at potentials matching with the redox wave of P-vio (Figure S8, Supporting Information), as expected from the mediated electron transfer configuration (see scheme in Figure 2, top right). However, only minor photocurrent responses were observed at those very negative potentials. The inherent presence of small gaps within the PSI-LB film can cause the leakage of P-Os chains during electrode preparation before the polymer is fully crosslinked. Consequently, the high-energy electrons exiting PSI may be redirected to P-Os instead of the electrode surface, cancelling out at least part of the generated photocurrent (see Figure 1d). As the applied potential is closer to the midpoint potential of P-vio, the driving force for the transfer of electrons between the reduced polymer-bound $vio^{+\bullet}$ and the electrode surface decreases. However, the potential difference between P-vio and P-Os remains constant (**Figure 4**a). Therefore, the short-circuiting pathway is more pronounced at the more negative applied potentials.

With the aim to minimize direct wiring of P-Os with the electrode surface or P-vio, an additional modification step with a nonredox active polymer (poly(ethylene glycol)diglycidyl ether, PEGDGE) was introduced to further optimize the bioelectrode, enabling to crosslink the immobilized PSI monolayer before deposition of the P-Os/GOx film. As shown in Figure 4b, relevant photocurrents could be now obtained at negative potentials, even close to the midpoint potential of P-vio. The minimized diversion of generated photoelectrons away from the electrode surface enabled a noticeably improved performance, with the photoanode providing photocurrents of up to 17.6 μA cm^{-2} at 200 mV vs SHE and delivering about 0.7 μA cm^{-2} at an applied potential of −300 mV vs SHE (Figure S9, Supporting Information). Note that no noticeable photocurrents could be recorded before with the biophotoelectrode at such negative applied potentials (see Figure 3a).

The long-term stability of the biophotoelectrode was also investigated. For this, the modified electrode was subjected to alternating dark and light periods while simultaneously recording the current output as a function of time. This enabled to compensate for changes in the baseline during the course of the measurement, allowing the determination of the photocurrent output as well as preventing possible secondary effects caused by heating of the sample after long illumination periods. As summarized in **Figure 5**, the biophotoelectrode exhibited a reasonable stability, retaining 75% of the initial photocurrent response after 60 min of the experiment and over 65% at the end of the measurement performed during 90 min. The decrease in activity over the long period of time may be attributed to a shift in the pH value near the bioelectrode surface as a result of accumulation of gluconic acid generated after the oxidation of glucose by GOx.

Despite the high performance of the developed biophotoanode, the presence of a pronounced oxidation wave at more positive applied potentials was evident, even in dark conditions (Figure 4b). This wave matched the midpoint potential of P-Os and was dependent on the concentration of glucose (Figure S10a, Supporting Information), indicating a direct communication between the P-Os film embedding GOx and the electrode surface. In order to exploit the true potential of the envisioned PSI-based biophotoanode for biophotovoltaic applications, able to provide high-energy electrons reaching the electrode surface at the potential of P-vio, the oxidation of P-Os via electron exchange with the electrode (see Figure 1b) must be prevented. However, a more rigorous blocking or crosslinking of the PSI-LB layer before modification with P-Os was not possible since it adversely affected the electrical communication with P_{700} and the integrity of the immobilized photosystems. Hence, the deposition of a much denser P-vio film was used as a means of fully blocking the electrical communication between P-Os and the electrode surface. It was essential to ensure the deposition of a sufficiently homogeneous polymer film that is compatible with the transfer and immobilization of the PSI-LB layer. The optimal procedure for this purpose was achieved

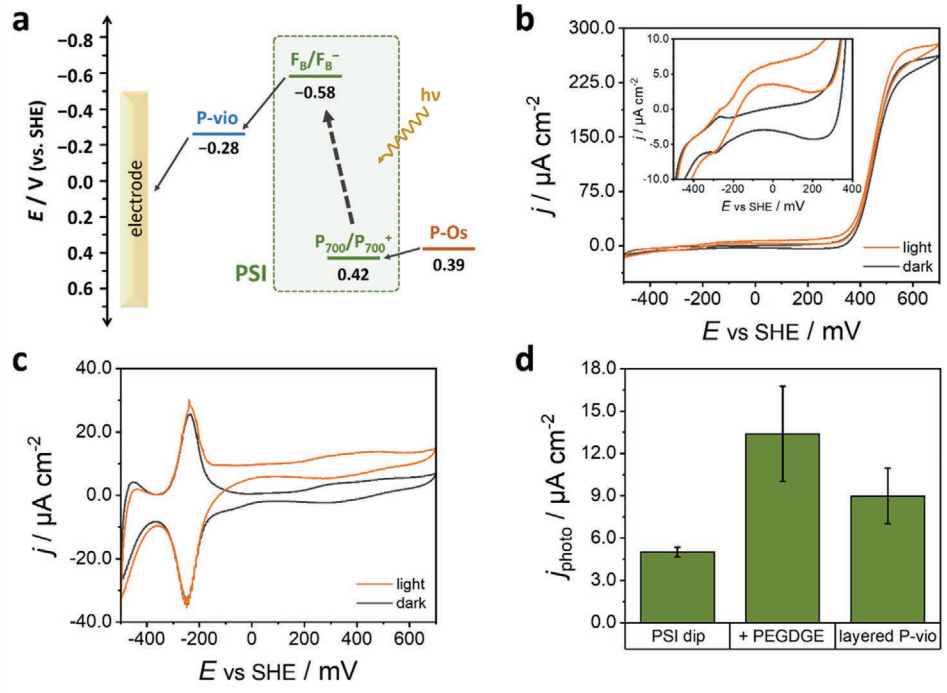

Figure 4. a) Simplified diagram highlighting the potential of the terminal redox centers at PSI and the midpoint potential of the redox polymers P-vio and P-Os. b) Cyclic voltammograms for a PSI-LB film over a P-vio-modified Au electrode, with an additional layer of the crosslinking agent PEGDGE, and with a top layer of GOx embedded in P-Os (Au/P-vio/PSI-LB/PEGDGE/P-Os/GOx). Electrolyte: Ar-saturated 0.1 M phosphate buffer, pH 7.0, containing 10×10^{-3} M glucose. Inset: Magnification of the recorded curves. c) Cyclic voltammograms obtained for a similar electrode as in (b) but fabricated using a layered deposition of P-vio (for details see main text). Electrolyte: Ar-saturated 0.1 M phosphate buffer, pH 7.0, containing 2×10^{-3} M glucose. d) Average photocurrent responses ($N = 3$ different electrodes prepared in the same manner) for Au/P-vio/PSI-LB/P-Os/GOx electrodes (PSI dip), Au/P-vio/PSI-LB/PEGDGE/P-Os/GOx electrodes (+PEGDGE), and an electrode fabricated using a layered deposition of P-vio (layered P-vio). $E_{app} = 200$ mV vs SHE. The error bars represent the standard deviation of the measurements.

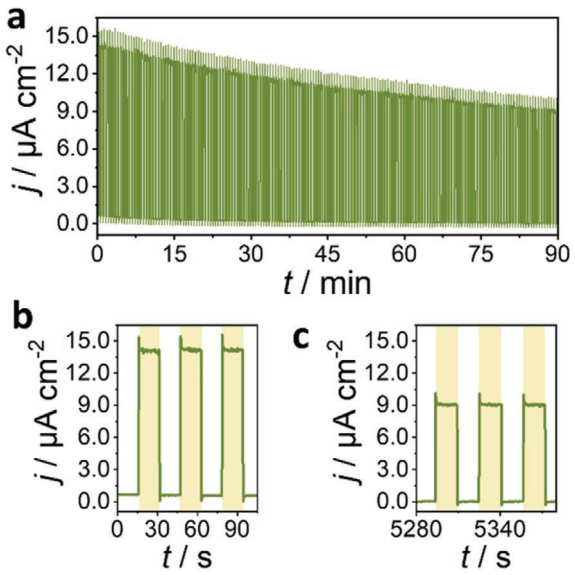

Figure 5. a) Photocurrent measurement for a Au/P-vio/PSI-LB/PEGDGE/P-Os/GOx electrode. Electrolyte: Ar-saturated 0.1 M phosphate buffer, pH 7.0, containing 10×10^{-3} M glucose. A magnification is also presented for b) the initial and c) final periods of the measurement. $E_{app} = 200$ mV vs SHE. Illumination with white light during the times indicated by the yellow-shaded regions. For clarity of the plot, the illumination periods are not indicated in panel (a).

by a sequential modification of the electrode with thinner P-vio layers (see the Experimental Section), leading to a finally increased coverage estimated to be (1.3 ± 0.8) nmol cm^{-2} ($N = 4$ different electrodes). As shown in Figure 4c, the light-induced response obtained in this case started at the redox potential of P-vio and did not present any noticeable contribution from the oxidation wave of P-Os as observed before (Figure S10b, Supporting Information). The photocurrent response attained with this bioelectrode was somewhat smaller in comparison with the bioelectrode fabricated using a rather thin P-vio film (Figure 4d), which could be attributed to comparatively diminished kinetics as a result of the thicker P-vio film necessary for preventing electrical wiring of P-Os. Still, the performance of the biophotoelectrode was notable and encouraged the implementation of a biophotovoltaic device.

2.4. Implementation of a Full Biophotovoltaic Cell

A gas-breathing biocathode was implemented, consisting of the enzymes GOx and horseradish peroxidase (HRP), coimmobilized onto a carbon cloth-based electrode material to complete the cell. The enzymes were tethered to the electrode by a functionalization step with 1-pyrenebutyric acid *N*-hydroxysuccinimide ester (PBSE), enabling the formation of an amide bond with primary amines exposed at the protein surface (**Figure 6**a).

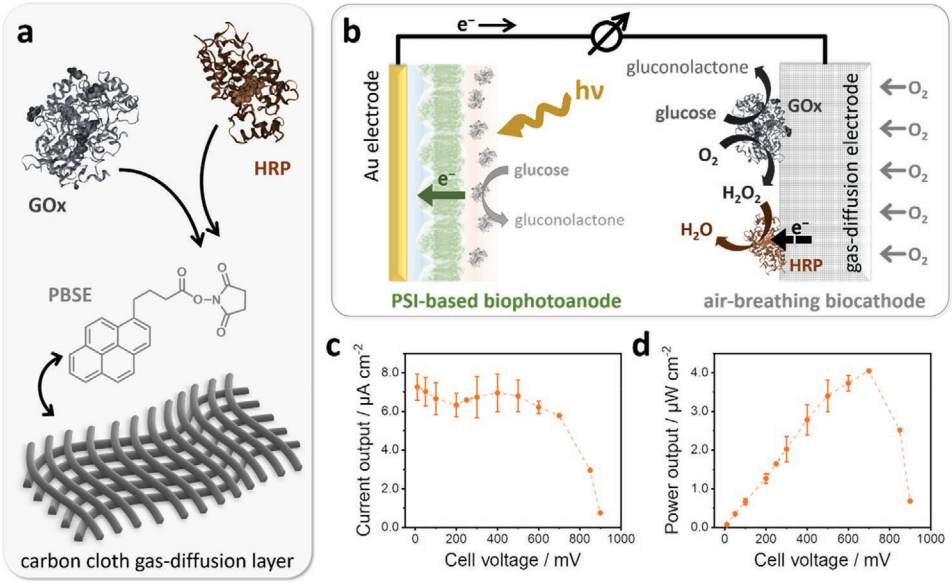

Figure 6. Fabrication and characterization of the complete biophotovoltaic cell. a) Schematic representation summarizing the biocathode fabrication. The carbon electrode material is first modified with PBSE by π–π stacking interactions. Subsequently, the enzymes GOx and HRP are attached to the electrode surface under the formation of amide bonds. b) Complete biophotovoltaic cell and operational details of the biocathode (elements not drawn to scale). The carbon cloth gas-diffusion electrode modified with GOx and HRP is operated in a passive air-breathing mode. GOx structure based on the PDB entry 3QVR;[29] HRP structure based on the PDB entry 1H5E.[34] c) Polarization curve and d) power curve obtained for the biophotovoltaic cell ($N = 2$ different sets of electrodes fabricated in the same manner). Electrolyte: Ar-purged 0.1 M phosphate buffer, pH 7.0, containing 3×10^{-3} M glucose. Single compartment cell. Illumination with white light. The error bars represent the standard deviation of the measurements.

In the presence of glucose in the electrolyte solution, GOx catalyzed the oxidation of glucose while reducing O_2 to H_2O_2. A direct electron transfer configuration between the electrode surface and the ferryl species $[(P)Fe^{IV} = O]^{+\bullet}$ (P represents the porphyrin π-system), known as compound I, at HRP allowed the high-potential biocatalytic reduction of the locally generated H_2O_2.[33] Because molecular oxygen was required for enabling the biocatalytic cascade reaction, a gas-diffusion layer was used as electrode to ensure a sufficient amount of O_2 reaching GOx under a simple passive air-breathing configuration (see Figure 6b, right). This was confirmed by the comparable electrochemical responses of the biocathode obtained when the electrolyte solution was open to ambient air or purged with an Ar stream for removal of dissolved O_2 (Figure S11a, Supporting Information). The GOx/HRP bioelectrode delivered substantially larger current densities than the PSI-based biophotoanode, even when using low glucose concentrations (Figure S11b, Supporting Information), which was essential for ensuring non-limiting conditions for the biophotoanode.

The biophotovoltaic cell was assembled by combining a PSI-based biophotoanode with the air-breathing biocathode in a single compartment cell (Figure 6b), and preliminarily characterized using the initially developed Au/P-vio/PSI-LB/P-Os/GOx biophotoelectrode. The obtained results (Figure S12, Supporting Information) revealed substantial current and power outputs for the biophotovoltaic cell. However, the maximum power output was reached at a rather low cell voltage of 300 mV, delivering only a minor power output for cell voltages larger than 500 mV (Figure S12b, Supporting Information). As discussed above, a direct communication between the P-Os/GOx film and the electrode surface was determining the output of this bioelectrode, causing a response that was practically independent of light and that was only as a result of mediated electron transfer between GOx and the electrode surface through the Os-complex-modified redox polymer (see Figure 1b). During the optimization of the biophotoelectrode for suppressing electrical communication between P-Os and the electrode surface, the different bioanodes fabricated were also investigated in combination with the GOx/HRP-based biocathode, assessing the power output in the dark. The power output correlated directly with the degree of electrical communication between P-Os and the electrode surface (Figure S13, Supporting Information). When the electrical communication between P-Os and the electrode was suppressed (Figure 4c), the power output in the dark was negligible, confirming the absence of any undesired competing pathways for the utilization of the high-energy electrons exiting PSI. The biophotovoltaic cell was then investigated under illumination, providing a large open-circuit voltage of about 960 mV, as expected for the combination of the two bioelectrodes. Moreover, the cell was able to deliver a maximum current density of (7.2 ± 0.7) μA cm^{-2} (Figure 6c) and exhibited a maximum power output of (3.7 ± 0.2) μW cm^{-2} at a voltage difference of 600 mV (Figure 6d).

3. Conclusions

Langmuir monolayers of photosystem I have been used as the basis for the fabrication of a PSI biophotoanode allowing control over the orientation of the biomolecule and a high density of photosynthetic protein complexes per unit area. In addition, the use of specifically designed redox polymers for interfacing

the immobilized photosystem provides an efficient mediated electronic communication at both terminal redox sites of PSI. This ensures wiring of the F_B Fe-S cluster with the electrode surface for the collection of the high-energy electrons as well as electron transfer with P_{700} at the other end of the protein complex. GOx, entrapped within the top modification layer, enables the oxidation of glucose as sacrificial electron donor, providing the electrons required for a sustained photocurrent generation. At the same time, the capability for consuming O_2 by reduced GOx provides a protective coating for the removal of traces of molecular oxygen that could otherwise compromise the performance of the biophotoelectrode. It is envisaged that the use of GOx could be substituted by other (bio)catalysts to perform alternative oxidation reactions of interest.

PSI is an outstanding and highly promising biomolecule for the fabrication of semi-artificial biophotovoltaic devices. However, it is of particular importance to consider the possible factors that can compromise the performance of a biophotoelectrode. By rationally designing the electrode architecture and optimizing the orientation of PSI, the short-circuiting of high-energy electrons is minimized and the direct oxidation of the electron donor at the electrode surface is prevented. The unprecedented possibility for minimizing the different factors that can compromise the bioelectrode performance (see Figure 1) translates into a biophotoanode that provides large photocurrents and an outstanding performance even at negative potentials. The anodic photocurrents obtained are substantially larger than those reported previously for PSI-based biophotoelectrodes comprised of a monolayer of PSI,[10,18,30,35] and even capable of outperforming bioelectrodes making use of PSI multilayers that have been fabricated in the absence of semiconductor materials.[11,13,25–27]

The capability of a PSI-based bioanode providing electrons at highly negative potentials could be exploited for the first time in the implementation of a complete biophotovoltaic cell. As a proof of concept, the cell was assembled by coupling the PSI bioanode with a GOx/HRP-based air-breathing biocathode. The use of the glucose-converting enzyme at both bioelectrodes simplifies the assembly and allows operation in a single compartment cell. Moreover, as the supply of O_2 is ensured by a gas-diffusion layer exposed to ambient air, the system can be simply powered by the presence of glucose and illumination with visible light. As a result, the biophotovoltaic cell delivers a considerable power output even at large cell voltages, reaching a maximum power output at a cell voltage about 400 mV higher than that obtained for the unoptimized assembly. The presented report highlights the requirements for a careful bioelectrode design considering all possible short-circuiting pathways and is paving the way for the development of advanced biophotoelectrodes able to exploit the true potential of PSI.

4. Experimental Section

Chemicals and Materials: All chemicals were of laboratory grade or higher and used as received. Potassium dihydrogen phosphate, dipotassium hydrogen phosphate trihydrate, calcium chloride, potassium chloride, potassium sulfate, dimethylformamide (DMF), D(−)-mannitol, and *n*-hexane were obtained from VWR Chemicals. Citric acid monohydrate was from J.T. Baker. Tris-HCl and D(+)-glucose monohydrate were purchased from AppliChem. Magnesium chloride, 2-(*N*-morpholino) ethanesulfonic acid (MES), and L(+)-ascorbic acid were from Carl Roth. *n*-Dodecyl *β*-D-maltoside was from GLYCON Biochemicals. Cysteamine, branched PEI (average M_n = 600 g mol^{-1}), hydrogen peroxide (30 wt%), PBSE, glucose oxidase (GOx, from *Aspergillus niger*, type X-S, 100–250 U mg^{-1} solid), and HRP (type VI-A, ≥250 U mg^{-1} solid) were from Sigma-Aldrich. PEGDGE (M_n = 400 g mol^{-1}) was from Polysciences. All solutions were prepared using deionized water (ρ = 18 MΩ cm) from a water purification system (SG Water).

Au wafers for the fabrication of photosystem-based bioelectrodes were obtained by coating Si(100) wafers (Wacker) with titanium as an adhesion layer and a gold layer using a metal vaporization setup. The carbon cloth-based gas-diffusion electrode (EQ-bcgdl-1400S-LD) for the fabrication of biocathodes was purchased from MTI Corporation.

Detailed descriptions about the synthesis and purification of the redox polymers can be found elsewhere: poly(3-azidopropyl methacrylate-*co*-butyl acrylate-*co*-glycidyl methacrylate)-viologen (P-vio);[20,21] poly(1-vinylimidazole-*co*-allylamine)-[Os(2,2'-bipyridine)$_2$Cl]Cl (P-Os).[32]

PSI has been isolated and purified from *Thermosynechococcus elongatus* BP-1 following previously reported protocols, enabling the collection of protein in the form of trimers[20,36] or monomers.[19,37]

Fabrication of Photosystem-Based Bioelectrodes: Prior to modification of the substrate, the Au wafers were cut to the desired size and cleaned using Piranha solution, consisting of concentrated H_2SO_4 and 30 wt% H_2O_2 in a 3 to 1 volumetric ratio. After rinsing thoroughly and drying under an Ar stream, a monolayer of cysteamine was formed on the Au surface by means of a potential pulse-assisted immobilization strategy. For this, the cleaned Au wafer was placed in an electrochemical cell with 1×10^{-3} M cysteamine in 10×10^{-3} M phosphate buffer (pH 7.4), containing 20×10^{-3} M K_2SO_4 and a series of potential pulses (–0.2 V for 10 ms, 0.5 V for 10 ms; potentials vs Ag/AgCl/3 M KCl) were applied for periods ranging between 2 and 5 min. Afterward, the modified Au surfaces were rinsed with water to remove any unbound cysteamine.

For the immobilization of the viologen-modified polymer, two different procedures were used. In a first approach, the modified Au electrode was immersed in an aqueous solution consisting of 8 µL P-vio (10 mg mL^{-1}) and 4 µL of PEI (2 vol% in water) in 2 mL H_2O, and incubated overnight. In a second approach, the modified Au electrode was immersed into a solution of 20 µL P-vio (10 mg mL^{-1}) and 5 µL PEI (2 vol% in water) in 2.5 mL H_2O, incubated for 60 min, and allowed to dry under ambient conditions for 30 min; this process was repeated four times. After the incubation period, the differently modified electrodes were thoroughly rinsed with water to remove any loosely bound material.

The deposition of PSI monolayers constituted by a mixture of the protein complexes in trimeric and monomeric forms was performed using an automated LB trough (KSV Instruments). In a similar way to the recent reports for the fabrication of PSI-LB monolayer-based bioelectrodes,[19,20] a Langmuir monolayer of PSI was formed by deposition of 2 µL of PSI trimers (9.0 mg$_{Chl}$ mL^{-1}) and 0.2 µL of PSI monomers (6.1 mg$_{Chl}$ mL^{-1}) onto an aqueous subphase consisting of 5×10^{-3} M phosphate buffer, pH 7.0, and subsequent compression of the structure formed at the air/water interface by means of two movable barriers. Once a surface pressure of 32 mN m^{-1} was reached, the formed monolayer was transferred onto the electrode previously modified with P-vio by dipping the substrate at a rate of 5 mm min^{-1} while keeping the surface pressure constant. Finally, the modified electrode was removed from the LB trough after opening the compression barriers to avoid interaction with remnant PSI. This situation led to the majority of PSI protein complexes with their F_B site directed toward the electrode surface. For control experiments with PSI in an opposite orientation, electrodes modified with P-vio were immersed into the subphase prior to formation of the PSI monolayer and pulled out at a rate of 5 mm min^{-1} for transfer of the monolayer onto the electrode surface (inverse transfer direction). All experiments were performed under dark conditions at 20 °C.

A top modification layer consisting of GOx embedded in the Os-complex-modified redox polymer (P-Os) was used to finalize the bioelectrode assembly. For this, a 10 or 25 µL aliquot of an aqueous solution of P-Os (0.5 mg mL^{-1}), the crosslinker PEGDGE (0.008 mg mL^{-1}), and GOx (5.0 mg mL^{-1}) was drop-casted over the modified electrode bearing the PSI monolayer and incubated at 4 °C in the dark overnight.

The sample was additionally incubated with 10 µL of 50×10^{-3} M Tris buffer (pH 9.0), containing 10×10^{-3} M $CaCl_2$, 10×10^{-3} M $MgCl_2$, and 100×10^{-3} M KCl to induce polymer collapse.[38] The fabrication process resulted in a modified surface of circular shape with dimensions of about 1 cm diameter. When indicated, the electrodes bearing the PSI-LB monolayer were additionally drop-coated with 50 µL of PEGDGE (0.04 mg mL^{-1}) and dried before modification with the P-Os layer.

Biocathode Fabrication: The microporous surface of the carbon cloth material used was modified with the enzymes HRP and GOx. For this, a piece of carbon cloth with an area of ≈3 cm × 3 cm was immersed into a solution of 10×10^{-3} M PBSE in DMF for 2 h. After that, the modified substrate was washed sequentially with DMF, *n*-hexane, and 5×10^{-3} M phosphate buffer (pH 7.0) to remove any loosely bound material and rests of organic solvents before modification with the enzymes. Finally, the resulting PBSE-functionalized carbon cloth was drop-coated with 60 µL of a mixture of GOx and HRP (2.5 mg mL^{-1} each) and incubated at 4 °C until dry. Before use, the electrode was rinsed with buffer solution to remove any unbound enzyme.

Electrochemical Characterization of Individual Bioelectrodes: A three-electrode setup was used, comprised of the modified electrode as working electrode, a Pt mesh as counter electrode, and a Ag/AgCl/3 M KCl reference electrode. For the characterization of PSI-modified electrodes, an electrochemical cell providing a circular exposed area of 0.246 cm^2 of the working electrode was used. As electrolyte solution, Ar-saturated 0.1 M phosphate buffer (pH 7.0) in the absence or presence of glucose was used, unless otherwise noted. The modified electrodes were investigated by performing cyclic voltammetry and photochronoamperometric measurements using a PGU-BI 100 potentiostat (IPS Jaissle). A He-Xe lamp (LC8 type 03, Hamamatsu Photonics) was used for illumination of the modified electrodes with white light at an incident power of 113 mW cm^{-2}. Typically, after a period of equilibration of the background current under dark conditions, the samples were illuminated for periods of 20 s at least two times at each applied potential. Long-term photocurrent measurements were performed at a constant applied potential of 200 mV vs SHE and switching between periods of dark and light (16 s each). For deriving the action spectrum, the PSI-modified electrode was polarized at a constant potential of 200 mV vs SHE by means of an Autolab PGSTAT12 (Metrohm Autolab) potentiostat and subjected to alternating dark and light periods (10 s each). Varying wavelengths ranging from 313 to 750 nm were used for the different illumination periods, as enabled by a monochromator setup (Instytut Fotonowy) placed immediately in front of a 150 W Xe lamp (Ushio) used as light source.

For the characterization of the GOx/HRP-modified gas-diffusion electrodes, cyclic voltammetry and amperometry at constant potential were performed with a PalmSens2 (PalmSens) potentiostat. The bioelectrode was used in passive air-breathing configuration (i.e., no forced gas flow through the gas-diffusion layer was applied). The modified side of the electrode was positioned facing the electrolyte solution and the back of it was open to the atmosphere. The electrolyte solution was either bubbled with Ar or remained equilibrated with ambient air, as indicated, and consisted of 0.1 M phosphate buffer (pH 7.0) in the absence or presence of glucose.

Spectroscopic Characterization of PSI: PSI absorption spectra were recorded in the range between 300 and 750 nm using a SHIMADZU UV-2450 UV–vis spectrophotometer using a dilution of 5 μg_{Chl} mL^{-1} in 20×10^{-3} M MES buffer pH 6.5, containing 10×10^{-3} M $MgCl_2$, 10×10^{-3} M $CaCl_2$, 500×10^{-3} M mannitol, and 0.03 wt% *n*-dodecyl β-D-maltoside.

Biophotovoltaic Measurements: A biophotovoltaic cell was assembled by combining the PSI-modified electrode as biophotoanode with the GOx/HRP-modified electrode as biocathode. The electrodes were placed in a single compartment cell, with the bioanode presenting an exposed circular area of 0.636 cm^2. An oversized biocathode was used, ensuring limiting conditions for the PSI-based bioelectrode, and was operated under a passive air-breathing configuration. The electrolyte solution consisted of 0.1 M phosphate buffer (pH 7.0) containing 3×10^{-3} M glucose, unless otherwise noted, and was continuously bubbled with Ar. Illumination of the bioanode was performed using white light at an incident power of ≈100 mW cm^{-2}. For the characterization of the biophotovoltaic cell, steady-state currents attained at different applied cell voltages were recorded and used for the calculation of polarization and power curves under illumination and dark conditions.

Supporting Information

Supporting Information is available from the Wiley Online Library or from the author.

Acknowledgements

P.W. and F.Z. contributed equally to this work. This work was supported by the Deutsche Forschungsgemeinschaft (DFG) in the framework of the Cluster of Excellence RESOLV (EXC 2033—project number 390677874) and the Research Training Group 2341 "MiCon" (Microbial Substrate Conversion) as well as the European Union's Horizon 2020 research and innovation programme under the Marie Skłodowska-Curie MSCA-ITN "Implantsens" (813006). P.W. is grateful for the financial support by the China Scholarship Council (CSC). The authors are grateful to Dr. Volker Hartmann for the isolation and purification of PSI trimers.

Open access funding enabled and organized by Projekt DEAL.

Conflict of Interest

The authors declare no conflict of interest.

Data Availability Statement

The data that support the findings of this study are available from the corresponding author upon reasonable request.

Keywords

biophotovoltaics, electrode materials, gas-diffusion electrodes, Langmuir–Blodgett films, photosystem I, redox polymers

Received: September 14, 2021
Revised: October 12, 2021
Published online: October 28, 2021

[1] a) E. Musazade, R. Voloshin, N. Brady, J. Mondal, S. Atashova, S. K. Zharmukhamedov, I. Huseynova, S. Ramakrishna, M. M. Najafpour, J.-R. Shen, B. D. Bruce, S. I. Allakhverdiev, *J. Photochem. Photobiol., C* **2018**, *35*, 134; b) M. T. Robinson, E. A. Gizzie, F. Mwambutsa, D. E. Cliffel, G. K. Jennings, *Curr. Opin. Electrochem.* **2017**, *5*, 211; c) A. H. Teodor, B. D. Bruce, *Trends Biotechnol.* **2020**, *38*, 1329.

[2] a) K. D. Wolfe, D. Dervishogullari, J. M. Passantino, C. D. Stachurski, G. K. Jennings, D. E. Cliffel, *Curr. Opin. Electrochem.* **2020**, *19*, 27; b) V. M. Friebe, R. N. Frese, *Curr. Opin. Electrochem.* **2017**, *5*, 126; c) S. K. Ravi, S. C. Tan, *Energy Environ. Sci.* **2015**, *8*, 2551; d) R. Tel-Vered, I. Willner, *ChemElectroChem* **2014**, *1*, 1778.

[3] K. Nguyen, B. D. Bruce, *Biochim. Biophys. Acta* **2014**, *1837*, 1553.

[4] O. Yehezkeli, R. Tel-Vered, D. Michaeli, I. Willner, R. Nechushtai, *Photosynth. Res.* **2014**, *120*, 71.

[5] H. Makita, G. Hastings, *Biochim. Biophys. Acta* **2016**, *1857*, 723.

[6] X. Fang, S. Kalathil, E. Reisner, *Chem. Soc. Rev.* **2020**, *49*, 4926.

[7] a) J. Z. Zhang, E. Reisner, *Nat. Rev. Chem.* **2020**, *4*, 6; b) W. Lubitz, M. Chrysina, N. Cox, *Photosyn. Res.* **2019**, *142*, 105.

[8] A. Zavafer, M. H. Cheah, W. Hillier, W. S. Chow, S. Takahashi, *Sci. Rep.* **2015**, *5*, 16363.
[9] A. Ruff, F. Conzuelo, W. Schuhmann, *Nat. Catal.* **2020**, *3*, 214.
[10] A. Efrati, C.-H. Lu, D. Michaeli, R. Nechushtai, S. Alsaoub, W. Schuhmann, I. Willner, *Nat. Energy* **2016**, *1*, 15021.
[11] O. Yehezkeli, R. Tel-Vered, D. Michaeli, R. Nechushtai, I. Willner, *Small* **2013**, *9*, 2970.
[12] A. Efrati, O. Yehezkeli, R. Tel-Vered, D. Michaeli, R. Nechushtai, I. Willner, *ACS Nano* **2012**, *6*, 9258.
[13] P. N. Ciesielski, C. J. Faulkner, M. T. Irwin, J. M. Gregory, N. H. Tolk, D. E. Cliffel, G. K. Jennings, *Adv. Funct. Mater.* **2010**, *20*, 4048.
[14] O. Yehezkeli, O. I. Wilner, R. Tel-Vered, D. Roizman-Sade, R. Nechushtai, I. Willner, *J. Phys. Chem. B* **2010**, *114*, 14383.
[15] P. N. Ciesielski, D. E. Cliffel, G. K. Jennings, *J. Phys. Chem. A* **2011**, *115*, 3326.
[16] a) D. Buesen, T. Hoefer, H. Zhang, N. Plumeré, *Faraday Discuss.* **2019**, *215*, 39; b) F. Zhao, N. Plumeré, M. M. Nowaczyk, A. Ruff, W. Schuhmann, F. Conzuelo, *Small* **2017**, *13*, 1604093.
[17] M. Kamran, J. D. Delgado, V. Friebe, T. J. Aartsma, R. N. Frese, *Biomacromolecules* **2014**, *15*, 2833.
[18] X. Yan, C. J. Faulkner, G. K. Jennings, D. E. Cliffel, *Langmuir* **2012**, *28*, 15080.
[19] P. Wang, A. Frank, F. Zhao, J. Szczesny, J. R. C. Junqueira, S. Zacarias, A. Ruff, M. M. Nowaczyk, I. A. C. Pereira, M. Rögner, F. Conzuelo, W. Schuhmann, *Angew. Chem., Int. Ed.* **2021**, *60*, 2000.
[20] F. Zhao, P. Wang, A. Ruff, V. Hartmann, S. Zacarias, I. A. C. Pereira, M. M. Nowaczyk, M. Rögner, F. Conzuelo, W. Schuhmann, *Energy Environ. Sci.* **2019**, *12*, 3133.
[21] J. Szczesny, N. Marković, F. Conzuelo, S. Zacarias, I. A. C. Pereira, W. Lubitz, N. Plumeré, W. Schuhmann, A. Ruff, *Nat. Commun.* **2018**, *9*, 4715.
[22] a) D. Jambrec, F. Conzuelo, A. Estrada-Vargas, W. Schuhmann, *ChemElectroChem* **2016**, *3*, 1484; b) D. Jambrec, M. Gebala, F. L. Mantia, W. Schuhmann, *Angew. Chem., Int. Ed.* **2015**, *54*, 15064.
[23] W. Zhu, R. Salles, M. Miyachi, Y. Yamanoi, T. Tomo, H. Takahashi, H. Nishihara, *Langmuir* **2020**, *36*, 6429.
[24] a) K. D. Wolfe, D. Dervishogullari, C. D. Stachurski, J. M. Passantino, G. K. Jennings, D. E. Cliffel, *ChemElectroChem* **2020**, *7*, 596; b) V. B. Shah, W. R. Henson, T. S. Chadha, G. Lakin, H. Liu, R. E. Blankenship, P. Biswas, *Langmuir* **2015**, *31*, 1675; c) Y. Yamanoi, N. Terasaki, M. Miyachi, Y. Inoue, H. Nishihara, *Thin Solid Films* **2012**, *520*, 5123; d) N. Terasaki, N. Yamamoto, T. Hiraga, Y. Yamanoi, T. Yonezawa, H. Nishihara, T. Ohmori, M. Sakai, M. Fujii, A. Tohri, M. Iwai, Y. Inoue, S. Yoneyama, M. Minakata, I. Enami, *Angew. Chem., Int. Ed.* **2009**, *48*, 1585; e) P. N. Ciesielski, A. M. Scott, C. J. Faulkner, B. J. Berron, D. E. Cliffel, G. K. Jennings, *ACS Nano* **2008**, *2*, 2465.
[25] S. Yang, M. T. Robinson, F. Mwambutsa, D. E. Cliffel, G. K. Jennings, *Electrochim. Acta* **2016**, *222*, 926.
[26] E. A. Gizzie, G. LeBlanc, G. K. Jennings, D. E. Cliffel, *ACS Appl. Mater. Interfaces* **2015**, *7*, 9328.
[27] E. Darby, G. LeBlanc, E. A. Gizzie, K. M. Winter, G. K. Jennings, D. E. Cliffel, *Langmuir* **2014**, *30*, 8990.
[28] P. Jordan, P. Fromme, H. T. Witt, O. Klukas, W. Saenger, N. Krauß, *Nature* **2001**, *411*, 909.
[29] P.-R. Kommoju, Z.-w. Chen, R. C. Bruckner, F. S. Mathews, M. S. Jorns, *Biochemistry* **2011**, *50*, 5521.
[30] A. Efrati, R. Tel-Vered, D. Michaeli, R. Nechushtai, I. Willner, *Energy Environ. Sci.* **2013**, *6*, 2950.
[31] D. Ciornii, M. Riedel, K. R. Stieger, S. C. Feifel, M. Hejazi, H. Lokstein, A. Zouni, F. Lisdat, *J. Am. Chem. Soc.* **2017**, *139*, 16478.
[32] F. Conzuelo, N. Marković, A. Ruff, W. Schuhmann, *Angew. Chem., Int. Ed.* **2018**, *57*, 13681.
[33] a) A. Ruff, J. Szczesny, N. Marković, F. Conzuelo, S. Zacarias, I. A. C. Pereira, W. Lubitz, W. Schuhmann, *Nat. Commun.* **2018**, *9*, 3675; b) A. Ruff, P. Pinyou, M. Nolten, F. Conzuelo, W. Schuhmann, *ChemElectroChem* **2017**, *4*, 890; c) W. Jia, S. Schwamborn, C. Jin, W. Xia, M. Muhler, W. Schuhmann, L. Stoica, *Phys. Chem. Chem. Phys.* **2010**, *12*, 10088.
[34] G. I. Berglund, G. H. Carlsson, A. T. Smith, H. Szöke, A. Henriksen, J. Hajdu, *Nature* **2002**, *417*, 463.
[35] R. K. Le, M. Raeeszadeh-Sarmazdeh, E. T. Boder, P. D. Frymier, *Langmuir* **2015**, *31*, 1180.
[36] A. Badura, D. Guschin, T. Kothe, M. J. Kopczak, W. Schuhmann, M. Rögner, *Energy Environ. Sci.* **2011**, *4*, 2435.
[37] O. Çoruh, A. Frank, H. Tanaka, A. Kawamoto, E. El-Mohsnawy, T. Kato, K. Namba, C. Gerle, M. M. Nowaczyk, G. Kurisu, *Commun. Biol.* **2021**, *4*, 304.
[38] T. Kothe, S. Pöller, F. Zhao, P. Fortgang, M. Rögner, W. Schuhmann, N. Plumeré, *Chem. - Eur. J.* **2014**, *20*, 11029.